Chemistry
A European
Journal

Chemistry Europe
European Chemical Societies Publishing

Accepted Article

Title: New Organometallic Ruthenium(II) Compounds Synergistically Show Cytotoxic, Antimetastatic and Antiangiogenic Activities for the Treatment of Metastatic Cancer

Authors: Yuchen Wang, Jiahui Jin, Liwei Shu, Tongyu Li, Siming Lu, Mohamed Kasim Mohamed Subarkhan, Chao Chen, and Hangxiang Wang

To be cited as: *Chem. Eur. J.* 10.1002/chem.202002970

Link to VoR: https://doi.org/10.1002/chem.202002970

WILEY-VCH

10.1002/chem.202002970

New Organometallic Ruthenium(II) Compounds Synergistically Show Cytotoxic, Antimetastatic and Antiangiogenic Activities for the Treatment of Metastatic Cancer

Yuchen Wang,[a,b] Jiahui Jin,[c] Liwei Shu,[a] Tongyu Li,[a] Siming Lu,[d] Mohamed Kasim Mohamed Subarkhan,[a] Chao Chen[e,] Hangxiang Wang[a,*]*

[a] The First Affiliated Hospital; Key Laboratory of Combined Multi-Organ Transplantation, Ministry of Public Health, School of Medicine, Zhejiang University, Hangzhou, 310003, PR China.

[b] Department of Chemical Engineering, Zhejiang University, Hangzhou, 310027, PR China

[c] Xingzhi College, Zhejiang Normal University, Jinhua, 321004, PR China

[d] Department of Laboratory Medicine, the First Affiliated Hospital, School of Medicine, Zhejiang University, Hangzhou, 310003, PR China.

[e] College of Life Sciences, Huzhou University, Huzhou, 313000, PR China.

Conflicts of Interest Disclosure Statement: *The authors declare no potential conflicts of interest.*

Corresponding Authors

**Hangxiang Wang (wanghx@zju.edu.cn)*

**Chao Chen (chenc@zjhu.edu.cn)*

Acknowledgements

The authors greatly acknowledge financial support from the Zhejiang Province Preeminence Youth Fund (Grant No. LR19H160002), the National Natural Science Foundation of China (Grant Nos. 81773193 and 81571799), and the National Science and Technology Major Project (Grant No. 2017ZX10203205).

Running title: *Ruthenium(II) compounds show efficacy against metastatic cancer*

Word count: 4206 *(main text)* ***Figures: 7 Tables: 1***

10.1002/chem.202002970

Abstract

In this study, we newly designed and synthesized a small library of ten structurally related C,N-cyclometalated ruthenium(II) complexes containing various pyridine-functionalized NHC ligand and chelating bipyridyl ligands (e.g., 2,2'-bipyridine, 5,5'-dimethyl-2,2'-bipyridine, and 1,10-phenanthroline (phen)). The complexes were well characterized by NMR, electrospray ionization-mass spectrometry, and single-crystal X-ray structure analyses. Among the new ruthenium(II) derivatives, we identified that the complex **Ru8** bearing bulky moieties (i.e., phen and pentamethyl benzene) had the most potent cytotoxicity against all tested cancer cell lines, generating dose- and cell line-dependent IC_{50} values at the range of 3.3-15.0 μM. More significantly, **Ru8** not only efficiently inhibited the antimetastasis process against invasion and migration of tumor cells but also exhibited potent antivascular effects by suppressing HUVEC cells migration and tube formation *in vitro* and blocking vessel generation *in vivo* (chicken chorioallantoic membrane model). In a metastatic A2780 tumor xenograft-bearing mouse model, administration of **Ru8** outperformed antimetastatic agent NAMI-A and clinically approved cisplatin in terms of antitumor efficacy and inhibition of metastases to other organs. Overall, these data provided compelling evidence that the new cyclometalated ruthenium complex **Ru8** is an attractive agent because of synergistically suppressing bulky tumors and metastasized tumor nudes. Therefore, the complex **Ru8** deserves further investigations.

KEYWORDS: ruthenium(II) complexes, cytotoxicity, antiangiogenesis, antimetastasis, cancer chemotherapy

10.1002/chem.202002970

Introduction

Chemotherapy is still regarded as the backbone for the management of patients with cancer and has improved the life expectancy of countless patients. Platinum-based drugs, including cisplatin, oxaliplatin, and carboplatin, have been extensively applied in the clinic for cancer chemotherapy [1]. However, the clinical efficacy of these platinum agents in patients has been greatly compromised by several drawbacks, including severe toxicities [2] (e.g., neurotoxicity and nephrotoxicity), inherent or acquired resistance and inability to impede tumor metastasis [3]. Clinically, metastatic cancer accounts for the majority of human deaths. Systemic administration of platinum drugs has produced local tumor control but is not capable of suppressing treatment escape pathways. For example, emerging evidence indicates that the repeated use of platinum chemotherapies is frequently associated with the dissemination of cancer cells, which eventually facilitates metastases to distant organs [4]. Towards the goal of addressing this medication challenge, new effective therapies that simultaneously combine cytotoxic, antimetastatic, and antiangiogenic activities are urgently needed and would be likely to provide long-term survival benefit to patients when clinically used.

Of the alternatives to platinum-based drugs, significant advances have been made with ruthenium-based agents that are appealing to exploration [5]. Compared to platinum drugs, ruthenium complexes generally show fewer side effects, no cross-resistance with cisplatin, and more diverse biological activities *in vitro* and *in vivo* [6]. Currently, several ruthenium(III) complexes (**Figure 1A**), including NAMI-A (imidazolium *trans*-[tetrachloro(dimethylsulfoxide)(1*H*-imidazole)ruthenate(III)]), which is effective against solid metastatic tumors [4], and KP1019 (indazolium *trans*-[tetrachlorobis(1*H*-indazole)ruthenium(III)]), which is used to combat resistant tumors [7], have entered clinical trials [8]. Unfortunately, these compounds have not yet shown the expected favorable clinical outcomes in cancer patients [9], stressing the need for the development of new metallodrugs. In addition to ruthenium(III) agents, ruthenium(II) arene complexes have attracted particular interest as anticancer drug candidates for clinical investigation due to certain advantages, including stability, aqueous solubility, structural diversity, and broad modes of action in biological systems [10]. Recently, a novel ruthenium (II) complex TLD1433, a photosensitizer, has entered the clinical trial for the treatment of non-muscle

10.1002/chem.202002970

invasive bladder cancer through the combination of photochemotherapy (PCT) and photodynamic therapy (PDT) [11]. Of the numerous ruthenium(II) compounds evaluated, some complexes [12] exhibited clinically relevant antimetastatic and antiangiogenic potential. It was reported that a series of ruthenium(II) complexes bearing the cinnamic acid moiety displayed desirable antimetastatic activities against migration and invasion in cancer cells [13]. We recently also demonstrated that tetranuclear ruthenium(II) arene complexes are promising anticancer agents that simultaneously span cytotoxic and antimetastatic mechanisms, as well as alleviated systemic toxicity in animals [14]. More intriguingly, ruthenium(II) complexes generally exhibit a lower systemic toxicity than other metallodrugs.

Cyclometallated ruthenium(II) complexes have recently demonstrated great potential as a new class of metallodrug candidates [9]. In these cycloruthenated complexes, the ligands are generally constructed with N- and C-donors. Compared to the ruthenium-N, the metal-to-ligand bond distances of ruthenium-C are significantly shorter, which endows the complexes with high stability in biological systems [15]. In addition, the cyclometalation decreases the valence charge of ruthenium(II) complexes and contributes to an increase in the lipophilicity and cellular uptake of the complexes [16]. As one of the well-documented cycloruthenated complexes, $[Ru(bpy)(phpy)(dppz)]^+$ (**Figure 1A**) showed superior activity against a panel of 2D cancer cell lines and 3D multicellular tumor spheroids compared to cisplatin [17]. Moreover, a cyclometallated ruthenium (II) complex RDC11 was recently demonstrated to possess promising antiangiogenic activity through the inhibition of the HIF1 pathway [18]. Furthermore, recent studies showed that cyclometallated ruthenium(II) polypyridyl complexes could be activated by near-infrared light irradiation, thereby serving candidates for PCT and PDT [19]. In these scaffolds, cyclometallated ligands were usually based on phenylpyridine and its derivatives, in which the structure diversity was limited due to the requirement of tedious synthesis for chemical derivatization of the phenylpridine ring. Accordingly, *N*-Heterocyclic carbenes (NHCs), in which the *N*-substituents of imidazole ring could be easily converted to various functional moieties , have attracted increasing interest. In addition, NHC ligands serve as excellent σ-donors, which may make the ruthenium complexes potentially stable [20]. Prompted by these studies, we designed novel effective NHC-coordinated cyclometallated ruthenium(II) complexes that spanned cytotoxic, antimetastatic and antiangiogenic mechanisms to address the therapeutic challenges

10.1002/chem.202002970

against metastatic cancer.

Towards this goal, we synthesized a small library of structurally relevant ruthenium(II) complexes, and their chemical structures were characterized by NMR spectra and X-ray crystallography studies. The cytotoxic activity in five cancer cell lines (including one cisplatin-resistant cancer cell) was assessed by the MTT assay, yielding dose-dependent IC_{50} values. Of the ten ruthenium complexes studied, **Ru8** showed the highest cytotoxic potency across distinct cancer cell lines. The unique feature of this agent is the ability to simultaneously kill cancer cells and impede metastasis, as well as angiogenesis in cell-based assays and *in vivo* studies. Our results showed that NHC-coordinated cyclometallated ruthenium(II) complexes possess multiple biological activities, thereby making them attractive for further investigations and clinical development.

Results

Synthesis of ruthenium(II) complexes

Ruthenium-NHC complexes **Ru1** and **Ru5** were synthesized according to the protocol [21] shown in **Figure 1B**. The reaction of the *in situ* generated silver-NHC complexes, a carbene transfer agent, with one equivalent of $[Ru(p\text{-cymene})Cl_2]_2$ and NH_4PF_6 in acetonitrile readily produced $[RuL1(CH_3CN)_4](PF_6)_2$ (**Ru1**) and $[RuL2(CH_3CN)_4](PF_6)_2$ (**Ru5**) in high yields (56-66%). The NMR spectra of **Ru1** and **Ru5** showed disappearance of the imidazolium C2-H protons. In addition, a substantial downfield shift of Ru-C carbon signal was observed for **Ru1** at δ 189.5 ppm and **Ru5** at 188.2 ppm, evidencing Ru-C bond formation. Furthermore, the peaks around 2.0 ppm ascribed to acetonitrile appeared in the purified complexes, suggesting successful coordination of acetonitrile ligand.

Motivated by the ease of compound synthesis, we further attempted to expand the library of ruthenium(II) derivatives. For this purpose, we reacted **Ru1** or **Ru5** with bidentate ligands (e.g., 2,2'-bipyridine (bpy), 5,5'-dimethyl-2,2'-bipyridine (dmbpy), and 1,10-phenanthroline (phen)) in reflux acetonitrile. This procedure efficiently yielded additional six ruthenium-NHC complexes (**Figure 1B**). Following a similar protocol, we prepared two chelate ruthenium-NHC complexes coordinating phen ligand $[RuL3(phen)(CH_3CN)_2](PF_6)_2$ (**Ru9**) and $[RuL4(phen)(CH_3CN)_2](PF_6)_2$ (**Ru10**), in which the R group was substituted to pentafluorophenyl and methyl, respectively, compared to **Ru4** and **Ru8**. The resulting

10.1002/chem.202002970

complexes **Ru1**-**10** were unambiguously characterized by NMR (^{1}H and ^{13}C) (**Figure S1**-**20**). The complexes were further dried and finally subjected to elemental analysis and electrospray ionization-mass (ESI-MS) spectrometry.

The stability of organometallic complexes plays an important role for their biological activities. Hence, choosing the complexes **Ru6** and **Ru8** as model complexes, we assessed the *in vitro* stability using UV-vis spectrometry. Upon incubation with different media (e.g., DMSO, PBS, and RPMI-1640 supplemented with 10% fetal bovine serum (FBS), almost negligible variation was observed for both complexes, manifesting that they were stable in solutions (**Figure S28**).

Single-crystal crystallography studies

Having these ruthenium(II) complexes in hand, we selected **Ru1**-**4** and **Ru8**-**10** for structural validation in the solid state by a single-crystal X-ray structure analysis. Single crystals suitable for X-ray crystallography studies were obtained by slowly diffusing diethyl ether into a freshly prepared and concentrated solution of the complexes in acetonitrile. The molecular structures created by the ORTEP (Oak Ridge thermal-ellipsoid plot) diagram are presented **Figure S21**-**27**. In the complex **Ru8**, the ruthenium(II) metal is hexa-coordinated by two ligands (i.e., L2 and phen) and two identical acetonitrile molecules in an octahedral geometry, which is consistent with the results of NMR characterization. Moreover, the carbene ligand, one acetonitrile ligand, and one nitrogen atom of phen are presented in the same equatorial plane, while the remaining coordinated nitrogen atoms of acetonitrile and chelating ligands lie on the axial positions (**Figure 2**). The planar aromatic structures are usually considered to have high affinities to intercalate into DNA double helix [22]. In addition, the cationic charge may readily cause **Ru8** to associate with negatively charged DNA [23]. The angles (N4-Ru-N5 and C6-Ru-N1) of the adjacent coordination atom are close to the right angle of 79.4 to 78.7°. Interestingly, the distance of ruthenium-N4 (2.126 Å) at the opposite position of the carbene ligand is slightly longer than the other four ruthenium-N bonds (2.044-2.079 Å), which is caused by the *trans*-effect of the strongly coordinated carbene ligand. In addition, single crystals of the complexes **Ru1**-**4** and **Ru9**-**10** were resolved by the same X-ray diffraction analysis, which possess similar structures with **Ru8** as shown in **Figure S21**-**27**.

10.1002/chem.202002970

In vitro cytotoxic activity

The ruthenium(II) complexes **Ru1**-**10** were tested for their cytotoxicity against the following cell lines: A549 (human lung cancer cells), A549/cisR (cisplatin-resistant human lung cancer cells), A2780 (human ovarian cancer cells), Huh-7 (human hepatocellular carcinoma cells), B16-F10 (mice melanoma cancer cells) and HUVEC (human umbilical vein endothelial cells). Following drug exposure for 72 h, cell viability was determined by the MTT assay. IC_{50} values (half-maximal inhibitory concentration) were extrapolated from the dose-response curves to determine the antiproliferative activity of the complexes, and these values are summarized in **Table 1**. Cisplatin, a widely used metallodrug in the clinic to treat cancer [24], was included as the control. Compared to the parent complexes **Ru1** or **Ru5**, incorporation of bpy, dmbpy, and phen moieties to the ruthenium metal center (i.e., complexes **Ru2**-**4** or **Ru6**-**8**) improved the cytotoxic activity in all tested cancerous cell lines. Specifically, the substitution with the phen motif significantly yielded better cytotoxicity than the others as evidenced by the reduced IC_{50} values. Interestingly, compared to complexes **Ru1**-**4** (containing phenyl substitution), **Ru5**-**8** (containing pentamethyl benzene ring) exhibited ~3- to 8-fold improvements in activity, manifesting the strong structure-activity relationships.

To further investigate how NHC ligands affect the cytotoxic potency of the compounds, we additionally synthesized **Ru9** and **Ru10**, in which pentafluorophenyl- and methyl-substituted NHC ligands were coordinated, respectively. Unfortunately, we failed to obtain more potent complexes according to the cytotoxicity assay data. Together, of the ten compounds studied, we identified that **Ru8** was the most potent against cancer cells showing comparable cytotoxic activity with cisplatin, and preferentially killed cancer cells over the non-cancerous cells due to the relatively high IC_{50} values in HUVEC. Very interestingly, in cisplatin-resistant A549/cisR cells, the resistance fold of **Ru8** was reduced to 2.2-fold, indicating the ability of reversing drug resistance (**Table 1**).

UV-vis spectrometric titration using **Ru8** was further exploited to examine whether the interactions between the ruthenium(II) complex and DNA occurred. Upon addition of calf thymus DNA (CT-DNA), the absorption peaks ascribed to **Ru8** centered at 344 nm gradually decreased (**Figure S29**). The result revealed the presence of interactions between **Ru8** and DNA base pairs exhibited superior cytotoxicity by interacting with DNA

10.1002/chem.202002970

base pairs. Moreover, the complex **Ru8** showed a favorable partition coefficient, which indicates good lipophilicity and can contribute to compound penetration across cell membranes (**Table S3**). Therefore, the potent cytotoxicity of **Ru8** may be attributable to the bulky volume of the chelating ligands, which favors high cellular uptake and strong interaction with DNA [17]. Due to the observed high activity in cell-based assays, we selected **Ru8** for evaluation in ensuing experiments.

Mode-of-action to induce cell death

We next evaluated cell proliferation inhibited by **Ru8** by detecting DNA synthesis using a 5-ethynyl-2'-deoxyuridine (EdU) assay. This method enables the incorporation of EdU, a thymidine analogue, into cellular DNA during replication [25]. Subsequently, labeling the EdU moiety with green fluorescent dye using the click reaction can be used to detect proliferating cells (**Figure 3A**). In untreated cells, a large fraction of proliferative cells (52.2±0.8%) was observed with green fluorescence. However, treatment with complex **Ru6** or **Ru8** significantly reduced the DNA replication ratios, showing a dose-dependent manner (**Figure 3C**). Notably, compared to **Ru6**, complex **Ru8** was more effective in blocking DNA replication over a wide range of drug concentrations. After treatment with 16 μM **Ru8**, DNA synthesis was almost terminated, and the cell proliferation rate was dramatically reduced to 7.7% (**Figure 3C**).

Next, the acridine orange/ethidium bromide (AO/EB) staining assay was conducted to validate cell apoptosis induced by **Ru8**. AO penetrates intact cell membranes and emits green fluorescence inside cells, while EB only enters apoptotic cells with damaged membranes and shows orange fluorescence [26]. As shown in **Figure 3B**, significant apoptosis was induced in A549 cells after treatment with **Ru8** for 48 h. Compared to **Ru6**, the apoptotic ratio was more profound in **Ru8**-treated cells, manifesting the higher cytotoxicity of complex **Ru8**. Upon treatment with **Ru8**, the number of total cells was distinctly reduced, whereas the apoptosis rate was markedly increased accompanied with morphological changes of tumor cells (**Figure 3D**). Thus, the AO/EB results were consistent with the IC_{50} values derived from the MTT assay.

Western blot was additionally performed to verify the mode of action of **Ru8** in cell proliferation inhibition and apoptosis induction. Upregulation of apoptosis-related proteins

10.1002/chem.202002970

(e.g., c-PARP, c-Caspase 3 and c-Caspase 9) confirmed that the cell apoptosis could be efficiently induced by **Ru8** *via* the classical apoptotic pathway (**Figure 3E**) [27]. In addition, G2/M phase transition-related proteins (e.g., cdc25c, cdc2 and cyclin B1) in **Ru8**-treated A2780 cells were significantly downregulated compared with that of **Ru6** treatment. These results indicate that the complex **Ru8** inhibited cell proliferation by arresting the cell cycle at G2/M phase through cdc25c/cdc2/cyclin B1 pathway [27]. Furthermore, downregulation of phosphorylated cdc25c (p-cdc25c) and cdc2 (p-cdc2) might be attributable to the total reduction of cdc25c and cdc2 proteins. Thus, the western blot results further confirmed the cellular mechanism of anticancer **Ru8** compound and evidenced that **Ru8** had higher activities than its structurally similar complex **Ru6** to inhibit cell proliferation and induce apoptosis.

We anticipate that the high antiproliferation and apoptosis inducing ability of **Ru8** may be attributable to the coordination of the phen ligand which could benefit the interactions with DNA. Furthermore, **Ru8** was more active than **Ru6**, which possesses a similar structure, further validating the importance of the coordination of the phen ligand.

In vitro antimetastatic activity

The migration and invasion of cancer cells are closely related to cancer metastasis to distant organs [28]. Upon destroying the extracellular matrix, cancer cells invade into lymph nodes and migrate into healthy tissues through circulation systems, thus promoting the progression of tumors [12, 29]. Initially, a scratch wound-healing assay was included here to evaluate the antimetastatic activity of **Ru8** using the highly metastatic human HCC Huh-7 cell line (**Figure 4A**). For comparison, NAMI-A, a potent antimetastatic agent undergoing clinical trials [30], was selected as a reference. Strikingly, exposure of cells to **Ru8** reduced cell migration, showing a dose-dependent suppression activity. The wound-healing ratio after incubation with 32 μM **Ru8** was reduced to 2.9% compared to untreated cells with 29.6% migrating cells (**Figure 4B**). Unexpectedly, NAMI-A yielded less antimetastatic activity than **Ru8**, suppressing the gap closure with 19.0% at 32 μM, which was comparable with the activity of **Ru8** at 4 μM (**Figure 4B**). To eliminate the influence of cytotoxicity, the wound-healing assay was further performed at low drug concentrations (e.g., IC_{10} and IC_{20}, **Table S4**) [31]. Encouragingly, **Ru8** remained active against migration as compared to

10.1002/chem.202002970

untreated cells. However, at the concentrations of IC_{10} or IC_{20}, NAMI-A failed to inhibit the gap closure in the cells (**Figure S30**).

A transwell assay was further conducted to investigate the efficacy of **Ru8** on Huh-7 cell invasion. The cell invasion ratio can be evaluated through counting the number of invaded cells stained with crystal violet [32]. Following treatment with **Ru8**, Huh-7 cell invasion was markedly reduced compared to untreated cells (**Figure 4C** and **4D**). NAMI-A only showed limited activity in preventing cell invasion even at relatively high concentration (i.e., 32 μM). Similarly, treatments of NAMI-A at low concentrations abolished the antiinvasive effect, whereas the number of invaded cells in the **Ru8**-treated group was remarkably diminished even at the IC_{10} and IC_{20} concentrations (**Figure S31**).

Inspired by these results, western blot was conducted to investigate the mechanisms of **Ru8** against Huh-7 cell metastasis. The enhancement of matrix metalloproteinases (MMPs) level and the dysregulation of epidermal growth factor receptor (EGFR) were closely associated with tumor metastasis [33]. Although the total expression of EGFR remained unaffected after **Ru8** treatment, the metastasis-relevant proteins, including MMP9 and p-EGFR, were significantly downregulated (**Figure 4E**). Furthermore, **Ru8** showed stronger inhibitory activity than NAMI-A. Thus, all data demonstrated the potential of using **Ru8** as a promising candidate to combat metastatic cancer.

In vitro and in vivo antiangiogenic activity

Endothelial cell migration plays a critical role in the development of tumor vessels; therefore, targeting this process is essential for antivascular therapy [34]. Thus, we selected human umbilical vein endothelial cells (HUVECs) as a model to examine the antiangiogenic activity of ruthenium(II) complexes. On the basis of the results described above, only **Ru8** was used in the ensuing studies. First, we used the wound-healing assay to evaluate the inhibition of migration of HUVECs *in vitro* after drug treatment. Cells were treated with serum-free culture medium in the case of proliferation. Treatment with **Ru8** suppressed the migration of HUVECs in a dose-dependent manner (**Figure 5A**). For example, the wound closure ratios were 24.4%, 28.3%, 16.0% and 7.7% after **Ru8** treatment at concentrations at 4, 8, 16, and 32 μM, respectively, whereas the wound closure ratio of untreated cells was 50.0% ($p < 0.01$, **Figure 5B**). More strikingly, the wound closure after **Ru8** treatment at low

10.1002/chem.202002970

concentrations was significantly inhibited, manifesting that **Ru8** serves as a potent antivascular agent (**Figure S32**). A tube formation assay was next performed to assess the antiangiogenic capability of **Ru8**. For this purpose, HUVECs were seeded on Matrigel containing proangiogenic factors. Robust capillary networks should form between single HUVECs. Interestingly, addition of **Ru8** at non-cytotoxic concentrations for 5 h resulted in dramatic suppression of tube formation (**Figure S33**). Treatment with **Ru8** at higher concentration (4 μM) for 2 h destroyed the tube-like structures, presenting only 16.5% of tube formation relative to untreated cells (100%, $p < 0.001$, **Figure 5C** and **5D**). Increasing the drug concentration further yielded pronounced activity. Hence, **Ru8** showed the potential to impair the formation of tubes, suggesting potent antiangiogenic activity.

Based on these *in vitro* results, we next used the chicken embryo chorioallantoic membrane (CAM) model to investigate if **Ru8** is capable of inhibiting angiogenesis and further blood vessel formation *in vivo* [35]. The CAM model is extensively used to analyze the antiangiogenic activity of drug candidates due to its rapid capillary proliferation. At embryo development day (EDD) 8, fertilized chicken egg tissues were topically treated with **Ru8** at concentrations ranging from 1.03 to 32 μM for 36 h. **Figure 6A** and **Figure S34** show typical images for CAM. The saline-treated CAM developed vascular networks densely and robustly. Following topical administration of **Ru8**, significant reduction of neovascularization on the chick embryo was observed. Moreover, the vessel formation was suppressed in a concentration-dependent manner. At the concentrations of 16 and 32 μM, **Ru8** substantially destroyed the capillary bed and reduced small vessels observed. The photographs and quantification of the number of branching points are shown in **Figure 6B**. Therefore, the *in vivo* CAM assays provided compelling evidence that **Ru8** inhibits angiogenesis, indicating an antivascular effect *in vivo*.

In vivo antitumor efficacy

Prior to the *in vivo* antitumor activity, we evaluated the maximum tolerated dose (MTD) of using the complex **Ru8**. The healthy ICR mice were intraperitoneally administered with **Ru8** at the doses of 5, 10 and 12.5 μmol/kg every day for five injections. Saline was included as a reference. As shown in **Figure S35**, the body weights of the mice receiving **Ru8** at 10 μmol/kg were stable, and no incidence of mouse death was observed during the experiment. Thus, we estimated that the MTD of **Ru8** was at least 10 μmol/kg (9.6 mg/kg).

10.1002/chem.202002970

However, the half lethal dose (LD_{50}) of cisplatin was reported to be less than 10 μmol/kg (3.0 mg/kg) with intraperitoneal injection every other day for 5 times [14]. Hence, we chose the tolerated dose at 2 μmol/kg of **Ru8** for further *in vivo* therapeutic assessment.

Ovarian cancer is the second most common cause of malignancy-associated deaths among women due to its high capacity of metastasis and invasion in patients [36]. We therefore assessed the therapeutic efficacy of using **Ru8** in a metastatic ovarian tumor model. This model was established in Balb/c nude mice by intraperitoneal implantation of human ovarian cancer A2780 cells [37]. When the cells were injected, they disseminated throughout the abdomen, and the tumor cells metastasized to the ovary. Following cell implantation, we intraperitoneally injected cisplatin, NAMI-A and **Ru8** at a dose of 2 μmol/kg to initiate therapy, and the daily injections lasted for one week. On day 21 postadministration, mice were sacrificed to examine tumors that localized in the abdomen and metastasized to ovaries. Obviously, mice treated with cisplatin, NAMI-A and **Ru8** showed local tumor control (**Figure 7A** and **7B**), as well as reduced metastatic tumor burdens in ovaries (**Figure 7C** and **7D**), compared to the DMSO-treated group. Noticeably, **Ru8** demonstrated significantly higher tumor inhibitory activity than the other treatments, showing an inhibition rate of ~91.4% for abdominal tumors ($p < 0.01$ versus cisplatin or NAMI-A treatments, **Figure 7B**). Further considering the metastatic potential of A2780 cells to ovaries, we weighed ovaries in each group to assess the antimetastatic capacity. Encouragingly, in **Ru8**-treated mice, the ovaries remained in the normal range comparable to healthy mice (**Figure 7C** and **7D**). In addition, the stable body weights of the mice supported the low toxicity and high tolerability of **Ru8** in animals (**Figure 7E**). Taken together, these results demonstrated that **Ru8** efficaciously inhibits tumor growth and suppresses metastases to other organs, making it promising for further clinical investigation as a multifunctional anticancer agent.

Discussion

The most extensively used metallodrugs such as cisplatin, oxaliplatin, and carboplatin are known to yield serious side effects, including peripheral neurotoxicity, nephrotoxicity, and hair loss [38]. In addition, although systemic administration of platinum agents could gain the local tumor control, this modality generally is not capable of addressing the issues of tumor recurrence and metastasis. Unfortunately, the majority (~90%) of cancer patients

10.1002/chem.202002970

died from metastasis in the clinic [39]. Therefore, it can be rationally envisioned that single agents synergistically combining anti-metastatic and cytotoxic activities could be promising to efficiently treat metastatic cancer. To address these unmet medical needs, numerous transition metal (e.g., Ru, Ag, Au, Cu, Ir, Ni, Pd, and Os) complexes have been investigated as alternative anticancer therapeutics [4, 40]. Among them, ruthenium complexes have attracted a surge of interest. Several ruthenium compounds have entered the clinical trials at the different stages [7, 41]. As a well-documented example, NAMI-A was demonstrated to suppress tumor metastasis but this agent was not sufficient to kill cancer cells simultaneously [42]. Consequently, there is a considerable incentive for the development of new generation metallotherapeutics that synergistically inhibit tumor metastasis and growth with reduced *in vivo* toxicity.

For this purpose, in the present study, we designed and synthesized a series of novel cyclometalated ruthenium(II) complexes (**Ru1**-**10**) coordinating with diverse NHC moieties and bipyridyl ligands (e.g., bpy, dmpy and phen). The geometrical structures of these complexes were validated *via* single-crystal X-ray analysis. Compared with many previously reported ruthenium complexes bearing polypyridyl ligands [16], the cyclometallated ligands endowed the overall molecules with higher stability and lipophilicity, which could facilitate cellular uptake and, thereby enhancing the cytotoxic activity [9, 43]. In contrast to the phenylpyridine (a widely used pharmacophore as cyclometallated ligands), the NHC moieties provided more chances in the development of structure diversity by converting the N-substituents of imidazole ring to various functional moieties [44].

The differences in IC_{50} values clearly revealed the structure-activity relationship for these compounds. For example, compared with the complexes **Ru1** and **Ru5**, their derivatives showed increased cytotoxicity due to the substitution of acetonitrile moieties with bpy, dmbpy and phen, which indicates that the incorporation of the planar aromatic chelating ligands with bulky volume may be contributable to their high activity [22a, 45]. Specifically, the substitution of the phen group rendered the complex **Ru8** with the strong ability to interact with DNA. Furthermore, we investigated the effect of NHC ligands and showed that the substitution of pentamethyl benzene moiety was beneficial to its cytotoxic activity. Of the ten complexes evaluated, **Ru8** was proven to be the most potent in inducing

10.1002/chem.202002970

cell apoptosis *via* the classical apoptotic pathway and inhibiting cell proliferation by arresting the cell cycle at G2/M phase against tested cancer cells [46].

In addition to the cytotoxic activity, **Ru8** was further validated to effectively impede metastasis of highly invasive Huh-7 cells through the inhibition of cell migration and invasion through downregulation of some metastasis-associated proteins (e.g., MMP9 and p-EGFR). Surprisingly, **Ru8** showed much stronger antimetastatic capability than NAMI-A, a potent antimetastatic agent confirmed in many *in vitro* and *in vivo* studies [47]. Furthermore, **Ru8** suppressed angiogenesis by inhibiting HUVEC migration and tube formation *in vitro*, as well as by reducing neovascularization in the CAM model. Thus, we hypothesized that the multifunctional **Ru8** could suppress the tumor progression by preventing the cancer cells metastasis to distant organs and interrupting the development of tumor vessels. To test this, we finally employed a metastatic ovarian tumor mouse model to evaluate the anticancer efficiency of **Ru8**. Animal studies showed that **Ru8** more potently inhibited the proliferation of tumor cells and suppressed the growth of metastases in ovaries compared with cisplatin and NAMI-A.

In summary, we newly synthesized ten C,N-cyclometalated ruthenium(II) complexes **Ru1**-**10** and the optimized complex **Ru8** not only showed potent cytotoxic activity but also effectively impeded tumor metastasis and angiogenesis, thereby synergistically enhancing the efficacy against metastatic cancer. Collectively, these results showed the effectiveness of novel cyclometalated ruthenium-NHC complexes, representing a promising scaffold for further clinical investigations.

Experimental Section

Materials and methods

[Ru(*p*-cymene)Cl_2]$_2$ and calf thymus DNA (CT-DNA) was purchased from Sigma-Aldrich (Shanghai, China). 2,2'-bipyridine (bpy), 5,5'-dimethyl-2,2'-bipyridine, and 1,10-phenanthroline were purchased from Tokyo Chemical Industry (Shanghai, China). Other reagents were purchased from J&K Chemical (Shanghai, China). All the solvents were purchased from Tianjin Yongda Chemical Reagent (Tianjin, China). All reactions were performed in dry solvents. ^{1}H and ^{13}C NMR spectra were recorded on a Bruker Avance-400 (400 MHz) spectrometer at 400 MHz for ^{1}H and 100 MHz for ^{13}C. Chemical shifts (δ) are

10.1002/chem.202002970

expressed in ppm downfield to TMS at δ = 0 ppm and coupling constants (*J*) are expressed in Hz. Elemental analyses were performed with a Flash EA 1112 from ThermoFinnigan. Mass spectrometry ESI-MS was recorded on an AB Triple TOF 5600 + System (AB SCIEX, Framingham, USA).

*Synthesis of [RuL1(CH_3CN)$_4$](PF_6)$_2$, (**Ru1**)*

Imidazolium salt HL1PF_6 (381 mg, 1 mmol) was dissolved in 25 mL of acetonitrile (CH_3CN) containing dispersive silver oxide (140 mg, 0.6 mmol) and then stirred at 50 °C for 24 h. After cooling the solution to room temperature, [Ru(*p*-cymene)Cl_2]$_2$ (306 mg, 0.5 mmol) was added to the mixture, which was then stirred for 2 h. The reaction mixture was then heated to reflux for 24 h after adding NH_4PF_6 (815 mg, 5 mmol). The mixture was filtered through vacuum filtration, concentrated under reduced pressure and precipitated by addition of diethyl ether (Et_2O) to obtain **Ru1**. Yield: 521 mg, 66%, light yellow solid. ^{1}H NMR (400 MHz, CD_3CN): δ 8.86-8.88 (m, 1H), 8.09-8.13 (m, 1H), 8.06-8.07 (d, *J* = 2.0, 1H), 7.83-7.85 (d, *J* = 4.0, 1H), 7.36-7.46 (m, 5H), 7.28-7.29 (d, *J* = 2.0, 2H), 5.63 (s, 2H), 2.25 (s, 3H), 2.10 (s, 6H), 1.96 (s, 3H). ^{13}C NMR (100 MHz, CD_3CN) δ 189.49 (Ru-C), 155.44, 153.45, 141.08, 137.41, 129.49, 128.62, 127.22, 125.28, 122.84, 118.46, 112.19, 53.41, 3.85, 3.63. Anal. Calcd for $C_{23}H_{25}F_{12}N_7P_2Ru$:C, 34.95; H, 3.19; N, 12.40. Found: C, 34.86; H, 3.16; N, 12.31. ESI-MS: calcd $C_{23}H_{25}F_{12}N_7P_2Ru$ for [M-CH_3CN-PF_6]$^+$ 605.0597, found 605.0598.

*Synthesis of [RuL1(bpy)(CH_3CN)$_2$](PF_6)$_2$, (**Ru2**)*

A mixture of **Ru1** (158 mg, 0.2 mmol) and the chelating ligand, 2,2'-bipyridine (byp) (32 mg, 0.2 mmol) in CH_3CN was refluxed and stirred for 24 h. The solution was evaporated under vacuum to obtain the crude product, which was further purified by flash column chromatography via dichloromethane-methanol (15:1). Yield: 97 mg, 56%, light yellow solid. ^{1}H NMR (400 MHz, CD_3CN) δ 8.90-8.92 (m, 1H), 8.07-8.11 (m, 1H), 7.90-7.91 (d, *J* = 2.0, 1H), 7.78-7.80 (d, *J* = 4.0, 1H), 7.43-7.46 (m, 1H), 6.70-6.71 (d, *J* = 2.0, 1H), 5.65 (s, 2H), 2.50 (s, 3H), 2.31 (s, 6H), 2.30 (s, 3H), 2.28 (s, 6H), 2.15 (s, 6H), 1.96 (s, 3H). ^{13}C NMR (100 MHz, CD_3CN) δ 188.17, 155.46, 153.44, 141.03, 136.85, 134.37, 134.02, 128.87, 127.14, 125.32, 124.25, 122.76, 122.72, 112.09, 49.58, 16.94, 16.65, 16.41, 4.14, 3.62.

10.1002/chem.202002970

Anal. Calcd for $C_{28}H_{35}F_{12}N_7P_2Ru$: C, 40.29; H, 3.15; N, 11.34. Found: C, 40.32; H, 3.14; N, 11.29. ESI-MS: calcd $C_{28}H_{35}F_{12}N_7P_2Ru$ for $[M\text{-}CH_3CN\text{-}PF_6]^+$ 675.1379, found 675.1362.

*Synthesis of $[RuL1(dmbpy)(CH_3CN)_2](PF_6)_2$, (**Ru3**)*

The synthetic protocol of **Ru3** was similar with **Ru2**. 5,5'-dimethyl-2,2'-bipyridine (dmbpy) (37 mg, 0.2 mmol) was used as the chelating ligand. Yield: 105 mg, 59%, orange solid. ^{1}H NMR (400 MHz, CD_3CN) δ 9.04 (s, 1H), 8.34-8.36 (d, *J* = 4.0, 1H), 8.13-8.15 (m, 2H), 8.10-8.12 (m, 1H), 7.89-7.93 (m, 1H), 7.79-7.81 (d, *J* = 4.0, 1H), 7.67-7.69 (m, 1H), 7.60 (s, 1H), 7.57-7.58 (d, *J* = 2.0, 1H), 7.38-7.45 (m, 6H), 7.01-7.05 (m, 1H), 5.69-5.83 (m, 2H), 2.62 (s, 3H), 2.24 (s, 3H), 2.13 (s, 3H), 1.97 (s, 3H). ^{13}C NMR (100 MHz, DMSO-d_6) δ 193.06, 155.71, 155.34, 155.04, 153.15, 151.19, 150.92, 140.41, 140.13, 138.99, 138.62, 137.79, 137.35, 129.26, 128.25, 127.71, 127.01, 126.42, 126.08, 123.58, 123.39, 123.02, 118.83, 112.49, 53.04, 18.73, 18.30, 4.44, 3.95. Anal. Calcd for $C_{31}H_{31}F_{12}N_7P_2Ru$: C, 41.71; H, 3.50; N, 10.98. Found: C, 41.52; H, 3.39; N, 10.79. ESI-MS: calcd $C_{31}H_{31}F_{12}N_7P_2Ru$ for $[M\text{-}PF_6]^+$ 748.1332, found 748.1342.

*Synthesis of $[RuL1(phen)(CH_3CN)_2](PF_6)_2$, (**Ru4**)*

The synthetic protocol of **Ru4** was similar with **Ru2**, and 1,10-phenanthroline (phen) (36 mg, 0.2 mmol) was used as the chelating ligand. Yield: 256 mg, 69%, orange solid. ^{1}H NMR (400 MHz, CD_3CN) δ 9.64-9.66 (m, 1H), 8.88-8.90 (m, 1H), 8.45-8.48 (m, 1H), 8.23-8.29 (m, 3H), 8.20 (s, 1H), 8.13-8.16 (d, *J* = 6.0, 1H), 7.80-7.88 (m, 2H), 7.62-7.63 (d, *J* = 2.0, 1H), 7.53-7.56 (m, 1H), 7.37-7.48 (m, 5H), 7.25-7.27 (m, 1H), 6.86-6.90 (m, 1H), 5.71-5.92 (m, 2H), 2.32 (s, 3H), 1.80 (s, 3H). ^{13}C NMR (100 MHz, CD3CN) δ 194.32, 157.38, 155.55, 152.49, 152.09, 148.98, 147.06, 140.35, 138.60, 137.60, 137.47, 131.50, 131.17, 129.56, 128.72, 128.37, 128.32, 127.53, 126.89, 125.84, 125.63, 122.64, 118.56, 112.27, 53.81, 4.22, 3.82. Anal. Calcd for $C_{31}H_{27}F_{12}N_7P_2Ru$: C, 41.90; H, 3.06; N, 11.03. Found: C, 41.72; H, 3.17; N, 11.12. ESI-MS: calcd $C_{31}H_{27}F_{12}N_7P_2Ru$ for $[M\text{-}PF_6]^+$ 744.1019, found 744.1024.

*Synthesis of $[RuL2(CH_3CN)_4](PF_6)_2$, (**Ru5**)*

The synthetic protocol of **Ru5** was similar with **Ru1**, and $HL2PF_6$ (451 mg, 1 mmol) was used as imidazolium salt. Yield: 482 mg, 56%, light yellow solid. ^{1}H NMR (400 MHz, CD_3CN) δ 8.90-8.92 (m, 1H), 8.07-8.11 (m, 1H), 7.90-7.91 (d, *J* = 2.0, 1H), 7.78-7.80 (d, *J* =

10.1002/chem.202002970

4.0, 1H), 7.43-7.46 (m, 1H), 6.70-6.71 (d, *J* = 2.0, 1H), 5.65 (s, 2H), 2.50 (s, 3H), 2.31 (s, 6H), 2.30 (s, 3H), 2.28 (s, 6H), 2.15 (s, 6H), 1.96 (s, 3H). ^{13}C NMR (100 MHz, CD_3CN) δ 188.17, 155.46, 153.44, 141.03, 136.85, 134.37, 134.02, 128.87, 127.14, 125.32, 124.25, 122.76, 122.72, 112.09, 49.58, 16.94, 16.65, 16.41, 4.14, 3.62. Anal. Calcd for $C_{28}H_{35}F_{12}N_7P_2Ru$: C, 39.08; H, 4.10; N, 11.39. Found: C, 39.03; H, 4.14; N, 11.41. ESI-MS: calcd $C_{28}H_{35}F_{12}N_7P_2Ru$ for $[M\text{-}CH_3CN\text{-}PF_6]^+$ 675.1379, found 675.1362.

*Synthesis of [RuL2(bpy)(CH$_3$CN)$_2$](PF$_6$)$_2$, (**Ru6**)*

The synthetic protocol of **Ru3** was similar with **Ru2**. A mixture of **Ru5** (172 mg, 0.2 mmol) and the chelating ligand, 2,2'-bipyridine (byp) (32 mg, 0.2 mmol) in CH_3CN was refluxed and stirred for 24 h. Then, the solution was evaporated under vacuum to obtain the crude product, and further purified by flash column chromatography. Yield: 123 mg, 66%, light orange solid. ^{1}H NMR (400 MHz, DMSO-*d*$_6$) δ 9.46-9.47 (m, 1H), 8.89-8.91 (d, *J* = 4.0, 1H), 8.69-8.71 (d, *J* = 6.0, 1H), 8.57 (s, 1H), 8.46-8.50 (m, 1H), 8.18-8.20 (d, *J* = 4.0, 1H), 8.00-8.09 (m, 4H), 7.39-7.43 (m, 2H), 7.16-7.19 (m, 1H), 7.07-7.08 (d, *J* = 2.0, 1H), 5.70-5.80 (m, 2H), 2.53 (s, 3H), 2.39 (s, 6H), 2.37 (s, 3H), 2.28 (s, 3H), 2.27 (s, 6H). ^{13}C NMR (100 MHz, DMSO-*d*$_6$) δ 191.74, 157.79, 156.68, 155.71, 154.95, 151.54, 151.18, 140.58, 139.81, 138.43, 136.01, 134.03, 133.29, 128.95, 128.59, 128.34, 127.78, 127.08, 124.58, 124.46, 123.43, 123.09, 118.61, 112.43, 49.07, 17.39, 17.18, 16.91, 4.26, 3.80. Anal. Calcd for $C_{34}H_{37}F_{12}N_7P_2Ru$: C, 43.69; H, 3.99; N, 10.49. Found: C, 43.61; H, 4.07; N, 10.43. ESI-MS: calcd $C_{34}H_{37}F_{12}N_7P_2Ru$ for $[M\text{-}PF_6]^+$ 790.1801, found 790.1799.

*Synthesis of [RuL2(dmbpy)(CH$_3$CN)$_2$](PF$_6$)$_2$, (**Ru7**)*

The synthetic protocol of **Ru7** was similar with **Ru6**. 5,5'-dimethyl-2,2'-bipyridine (dmbpy) (37 mg, 0.2 mmol) was used as the chelating ligand. Yield: 110 mg, 57%, orange solid. ^{1}H NMR (400 MHz, DMSO-*d*$_6$) δ 9.18-9.19 (d, *J* = 2.0, 1H), 8.73-8.75 (d, *J* = 4.0, 1H), 8.54-8.57 (m, 2H), 8.28-8.30 (m, 1H), 8.19-8.20 (d, *J* = 2.0, 1H), 8.00-8.04 (m, 1H), 7.86-7.88 (m, 1H), 7.66 (s, 1H), 7.44-7.46 (m, 1H), 7.16-7.20 (m, 1H), 7.02-7.03 (d, *J* = 2.0, 1H), 5.69-5.78 (m, 2H), 2.68 (s, 3H), 2.54 (s, 3H), 2.38 (s, 6H), 2.37 (s, 3H), 2.29 (s, 3H), 2.28 (s, 6H), 2.22 (s, 3H). ^{13}C NMR (100 MHz, DMSO-*d*$_6$) δ 189.92, 153.70, 153.34, 152.91, 151.16, 149.12, 148.83, 138.33, 138.07, 136.95, 136.60, 135.42, 133.99, 131.90, 131.23, 126.56, 126.08, 124.91, 121.55, 121.36, 121.01, 120.92, 116.59, 110.41, 47.03, 16.69, 16.34, 15.29, 15.08, 14.76, 2.25, 1.75. Anal. Calcd for $C_{36}H_{41}F_{12}N_7P_2Ru$: C, 44.91; H, 4.29;

N, 10.18. Found: C, 44.69; H, 4.33; N, 10.07. ESI-MS: calcd $C_{36}H_{41}F_{12}N_7P_2Ru$ for $[M\text{-}PF_6]^+$ 818.2114, found 818.2082.

*Synthesis of [RuL2(phen)(CH$_3$CN)$_2$](PF$_6$)$_2$, (**Ru8**)*

The synthetic protocol of **Ru3** was similar with **Ru6**. 1,10-phenanthroline (phen) (36 mg, 0.2 mmol) was used as the chelating ligand. Yield: 125 mg, 65%, orange solid. ^{1}H NMR (400 MHz, DMSO-*d*$_6$) δ 9.86-9.87 (m, 1H), 9.11-9.13 (m, 1H), 8.67-8.69 (d, *J* = 4.0, 1H), 8.62 (s, 1H), 8.42-8.47 (m, 3H), 8.30-8.33 (d, *J* = 6.0, 1H), 8.18-8.20 (d, *J* = 4.0, 1H), 7.94-7.98 (m, 1H), 7.75-7.79 (m, 1H), 7.29-7.30 (d, *J* = 2.0, 1H), 7.14-7.15 (d, *J* = 2.0, 1H), 6.99-7.02 (t, *J* = 6.0, 1H), 5.77-5.89 (m, 2H), 2.60 (s, 3H), 2.44 (s, 6H), 2.29 (s, 9H), 2.25 (s, 3H). ^{13}C NMR (100 MHz, DMSO-*d*$_6$) δ 191.55, 157.46, 154.97, 152.51, 151.44, 149.47, 148.14, 146.31, 141.17, 140.47, 138.79, 137.51, 136.01, 134.09, 133.32, 130.93, 130.61, 129.08, 128.42, 128.28, 128.08, 127.24, 126.66, 126.42, 123.53, 122.97, 118.69, 112.35, 49.12, 17.41, 17.21, 16.96, 4.30, 3.78. Anal. Calcd for $C_{36}H_{37}F_{12}N_7P_2Ru$: C, 45.10; H, 3.89; N, 10.23. Found: C, 45.44; H, 3.93; N, 10.32. ESI-MS: calcd $C_{36}H_{37}F_{12}N_7P_2Ru$ for $[M\text{-}PF_6]^+$ 814.1801, found 814.1811.

*Synthesis of [RuL3(phen)(CH$_3$CN)$_2$](PF$_6$)$_2$, (**Ru9**)*

Ru9 was synthesized by using HL3PF$_6$ as imidazolium salt. A mixture of HL3PF$_6$ (235 mg, 0.5 mmol) and Ag_2O (65 mg, 0.3 mmol) in acetonitrile was stirred at 50 °C for 24 h. After cooling to room temperature, [Ru(*p*-cymene)Cl$_2$]$_2$ (153 mg, 0.25 mmol) was added and stirred for 2 h. After that, NH_4PF_6 (408 mg, 2.5 mmol) was added and the mixture was heated to reflux for 24 h. The resulting mixture was directly added by the chelating ligand 1,10-phenanthroline (phen) (90 mg, 0.5 mmol) without purification. The solution was further refluxed and stirred for another 24 h. After cooling to room temperature, the solution was evaporated under vacuum to obtain the crude product of **Ru9**, which was further purified by flash column chromatography. Yield: 298 mg, 61%, orange solid. ^{1}H NMR (400 MHz, DMSO-*d*$_6$) δ 9.82-9.84 (d, *J* = 4.0, 1H), 9.10-9.12 (d, *J* = 4.0, 1H), 8.76 (s, 1H), 8.66-8.68 (d, *J* = 4.0, 1H), 8.42-8.47 (m, 2H), 8.29-8.34 (m, 2H), 8.17-8.19 (d, *J* = 4.0, 1H), 7.96-8.00 (t, *J* = 8.0, 1H), 7.81 (s, 1H), 7.69-7.73 (m, 1H), 7.27-7.29 (d, *J* = 4.0, 1H), 7.00-7.03 (t, *J* = 6.0, 1H), 5.96 (s, 2H), 2.54 (s, 3H), 2.23 (s, 3H). ^{13}C NMR (100 MHz, DMSO-*d*$_6$) δ 193.30, 157.34, 154.83, 152.53, 151.51, 148.07, 146.22, 140.52, 138.85, 137.60, 130.94, 130.60, 128.40, 128.27, 127.88, 127.25, 126.18, 124.45, 123.13, 119.50, 112.46, 41.65, 4.23, 3.87.

10.1002/chem.202002970

Anal. Calcd for $C_{31}H_{22}F_{17}N_7P_2Ru$: C, 38.05; H, 2.27; N, 10.02. Found: C, 38.25; H, 2.22; N, 9.98. ESI-MS: calcd $C_{31}H_{22}F_{17}N_7P_2Ru$ for $[M\text{-}PF_6]^+$ 834.0548, found 834.0525.

*Synthesis of [RuL4(phen)(CH$_3$CN)$_2$](PF$_6$)$_2$, (**Ru10**)*

The synthetic protocol of **Ru7** was similar with **Ru9**, and $HL4PF_6$ (160 mg, 0.5 mmol) was used as imidazolium salt. Yield: 289 mg, 70%, orange solid. ^{1}H NMR (400 MHz, DMSO-d_6) δ 9.80-9.81 (m, 1H), 9.08-9.10 (m, 1H), 8.67-8.68 (d, *J* = 2.0, 1H), 8.63-8.65 (m, 1H), 8.43-8.45 (m, 2H), 8.27-8.29 (d, *J* = 4.0, 1H), 8.16-8.19 (m, 2H), 8.00-8.01 (d, *J* = 2.0, 1H), 7.94-7.99 (m, 1H), 7.69-7.73 (m, 1H), 7.26-7.27 (d, *J* = 2.0, 1H), 6.97-7.00 (m, 1H), 4.53-4.58 (m, 2H), 2.55 (s, 3H), 2.29 (s, 3H), 1.57-1.61 (t, *J* = 8.0, 3H). ^{13}C NMR (100 MHz, DMSO-d_6) δ 189.38, 154.70, 152.84, 150.40, 149.40, 146.08, 144.14, 138.31, 136.60, 135.36, 128.79, 128.50, 126.32, 126.11, 125.95, 125.08, 124.54, 124.23, 123.35, 120.78, 116.16, 110.11, 43.41, 14.92, 2.20, 1.57. Anal. Calcd for $C_{26}H_{25}F_{12}N_7P_2Ru$: C, 37.78; H, 3.05; N, 11.86. Found: C, 37.70; H, 3.11; N, 11.84. ESI-MS: calcd $C_{26}H_{25}F_{12}N_7P_2Ru$ for $[M\text{-}PF_6]^+$ 682.0862, found 682.0849.

X-ray Crystallography

Single crystal diffraction analysis was performed for **Ru1**-**4** and **Ru8**-**10** using a Siemens Smart-CCD area-detector diffractometer with Mo Kα radiation (λ = 0.710 73 Å) in ω scan mode. Absorption was corrected by multiscan. Oxford Diffraction CrysAlisPro software was employed to collect data. Structures were clearly solved by direct methods and refined by full-matrix least-squares on F^2 using the *SHELXTXL* package. In addition, nonhydrogen atoms were defined by full-matrix least-squares on F^2 with anisotropic temperature factors. Hydrogen atoms were regularly positioned based on various distances of C-H as follows: 0.95 Å for aromatic CH; 0.99 Å for CH_2; and 0.98 Å for CH_3 on a riding model with $U_{iso}(H) = -1.2–1.5U_{eq}(C)$. All data were calculated and shown in **Table S1** and **Table S2**.

Supporting Information

The supporting information contains experimental sections, ^{1}H and ^{13}C NMR spectra for the complexes **Ru1**-**10**, ORTEP diagrams for the complexes, and *in vitro* and *in vivo* characterizations for the complexes. The tables show crystallographic data, lipophilicity and cytotoxicity values for the complexes.

References

[1] T. C. Johnstone, K. Suntharalingam and S. J. Lippard, *Chem. Rev.* **2016**, *116*, 3436-3486.

[2] a) M. R. Trendowski, O. El Charif, P. C. Dinh, L. B. Travis and M. E. Dolan, *Clin. Cancer Res.* **2019**, *25*, 1147-1155; b) Y. Yang, L. Guo, Z. Tian, X. Ge, Y. Gong, H. Zheng, S. Shi and Z. Liu, *Organometallics* **2019**, *38*, 1761-1769.

[3] M. Ohmichi, J. Hayakawa, K. Tasaka, H. Kurachi and Y. Murata, *Trends Pharmacol. Sci.* **2005**, *26*, 113-116.

[4] A. Bergamo and G. Sava, *Chem. Soc. Rev.* **2015**, *44*, 8818-8835.

[5] a) R. G. Kenny and C. J. Marmion, *Chem. Rev.* **2019**, *119*, 1058-1137; b) W. Ma, L. Guo, Z. Tian, S. Zhang, X. He, J. Li, Y. Yang and Z. Liu, *Dalton Trans.* **2019**, *48*, 4788-4793.

[6] S. Thota, D. A. Rodrigues, D. C. Crans and E. J. Barreiro, *J. Med. Chem.* **2018**, *61*, 5805-5821.

[7] C. G. Hartinger, M. A. Jakupec, S. Zorbas-Seifried, M. Groessl, A. Egger, W. Berger, H. Zorbas, P. J. Dyson and B. K. Keppler, *Chem. Biodiversity* **2008**, *5*, 2140-2155.

[8] J. Li, Z. Tian, X. Ge, Z. Xu, Y. Feng and Z. Liu, *Eur. J. Med. Chem.* **2019**, *163*, 830-839.

[9] L. Zeng, P. Gupta, Y. Chen, E. Wang, L. Ji, H. Chao and Z. S. Chen, *Chem. Soc. Rev.* **2017**, *46*, 5771-5804.

[10] Q. Du, L. Guo, M. Tian, X. Ge, Y. Yang, X. Jian, Z. Xu, Z. Tian and Z. Liu, *Organometallics* **2018**, *37*, 2880-2889.

[11] a) G. Golbaghi and A. Castonguay, *Molecules* **2020**, *25*, 265; b) S. Monro, K. L. Colon, H. Yin, J. Roque, 3rd, P. Konda, S. Gujar, R. P. Thummel, L. Lilge, C. G. Cameron and S. A. McFarland, *Chem. Rev.* **2019**, *119*, 797-828.

[12] W. L. Kwong, K. Y. Lam, C. N. Lok, Y. T. Lai, P. Y. Lee and C. M. Che, *Angew. Chem., Int. Ed.* **2016**, *55*, 13524-13528.

[13] A. E. Graminha, J. Honorato, L. L. Dulcey, L. R. Godoy, M. F. Barbosa, M. R. Cominetti, A. C. Menezes and A. A. Batista, *J. Inorg. Biochem.* **2020**, *206*, 111021.

[14] M. K. M. Subarkhan, L. L. Ren, B. B. Xie, C. Chen, Y. C. Wang and H. X. Wang, *Eur. J. Med. Chem.* **2019**, *179*, 246-256.

[15] F. Cisnetti and A. Gautier, *Angew. Chem., Int. Ed.* **2013**, *52*, 11976-11978.

[16] F. E. Poynton, S. A. Bright, S. Blasco, D. C. Williams, J. M. Kelly and T. Gunnlaugsson, *Chem. Soc. Rev.* **2017**, *46*, 7706-7756.

[17] H. Y. Huang, P. Y. Zhang, B. L. Yu, Y. Chen, J. Q. Wang, L. N. Ji and H. Chao, *J. Med. Chem.* **2014**, *57*, 8971-8983.

[18] V. Vidimar, C. Licona, R. Ceron-Camacho, E. Guerin, P. Coliat, A. Venkatasamy, M. Ali, D. Guenot, R. Le Lagadec, A. C. Jung, J. N. Freund, M. Pfeffer, G. Mellitzer, G. Sava and C. Gaiddon, *Cancer Lett.* **2019**, *440-441*, 145-155.

[19] a) B. Peña, A. David, C. Pavani, M. S. Baptista, J.-P. Pellois, C. Turro and K. R. Dunbar, *Organometallics* **2014**, *33*, 1100-1103; b) J. A. Solis-Ruiz, A. Barthe, G. Riegel, R. O. Saavedra-Diaz, C. Gaiddon and R. Le Lagadec, *J. Inorg. Biochem.* **2020**, *208*, 111080.

[20] C. Yang, F. Mehmood, T. L. Lam, S. L. Chan, Y. Wu, C. S. Yeung, X. Guan, K. Li, C. Y. Chung, C. Y. Zhou, T. Zou and C. M. Che, *Chem. Sci.* **2016**, *7*, 3123-3136.

[21] C. Chen, C. Lu, Q. Zheng, S. Ni, M. Zhang and W. Chen, *Beilstein J. Org. Chem.* **2015**, *11*, 1786-1795.

[22] a) S. J. Lippard, P. J. Bond, K. C. Wu and W. R. Bauer, *Science* **1976**, *194*, 726-728; b) S. Arnott, P. J. Bond and R. Chandrasekaran, *Nature* **1980**, *287*, 561-563.

[23] M. R. Gill and J. A. Thomas, *Chem. Soc. Rev.* **2012**, *41*, 3179-3192.

[24] X. Wang, X. Wang and Z. Guo, *Acc. Chem. Res.* **2015**, *48*, 2622-2631.

[25] H. X. Wang, L. Q. Zhou, K. Xie, J. P. Wu, P. H. Song, H. Y. Xie, L. Zhou, J. L. Liu, X. Xu, Y. Q. Shen and S. S. Zheng, *Theranostics* **2018**, *8*, 3949-3963.

[26] K. Xie, S. S. Song, L. Q. Zhou, J. Q. Wan, Y. T. Qiao, M. Wang, H. Y. Xie, L. Zhou, S. S. Zheng and H. X. Wang, *Int. J. Pharm.* **2019**, *556*, 159-171.

[27] B. Xie, J. Wan, X. Chen, W. Han and H. Wang, *Mol. Cancer Ther.* **2020**, *19*, 822-834.

[28] H. Hamidi and J. Ivaska, *Nat. Rev. Cancer* **2018**, *18*, 532-547.

[29] X. Ge, S. Chen, X. Liu, Q. Wang, L. Gao, C. Zhao, L. Zhang, M. Shao, X. A. Yuan, L. Tian and Z. Liu, *Inorg. Chem.* **2019**, *58*, 14175-14184.

[30] D. Cirri, M. G. Fabbrini, A. Pratesi, L. Ciofi, L. Massai, T. Marzo and L. Messori, *Biometals* **2019**, *32*, 813-817.

[31] B. T. Elie, J. Fernandez-Gallardo, N. Curado, M. A. Cornejo, J. W. Ramos and M. Contel, *Eur. J. Med. Chem.* **2019**, *161*, 310-322.

[32] F. U. Rahman, M. Z. Bhatti, A. Ali, H. Q. Duong, Y. Zhang, X. J. Ji, Y. J. Lin, H. Wang, Z. T. Li and D. W. Zhang, *Eur. J. Med. Chem.* **2018**, *157*, 1480-1490.

[33] a) M. Egeblad and Z. Werb, *Nat Rev Cancer* **2002**, *2*, 161-174; b) S. Kalyankrishna and J. R. Grandis, *J. Clin. Oncol.* **2006**, *24*, 2666-2672.

[34] R. S. Kerbel, *Science* **2006**, *312*, 1171-1175.

[35] D. D. Sun, Y. N. Liu, Q. Q. Yu, Y. H. Zhou, R. Zhang, X. J. Chen, A. Hong and J. Liu, *Biomaterials* **2013**, *34*, 171-180.

[36] S. Lheureux, M. Braunstein and A. M. Oza, *Ca-Cancer J. Clin.* **2019**, *69*, 280-304.

[37] L. Shu, L. Ren, Y. Wang, T. Fang, Z. Ye, W. Han, C. Chen and H. Wang, *Chem. Commun.* **2020**, *56*, 3069-3072.

[38] L. B. Travis, S. D. Fossa, H. D. Sesso, R. D. Frisina, D. N. Herrmann, C. J. Beard, D. R. Feldman, L. C. Pagliaro, R. C. Miller, D. J. Vaughn, L. H. Einhorn, N. J. Cox, M. E. Dolan and G. Platinum Study, *J. Natl. Cancer Inst.* **2014**, *106*, 44-54.

[39] K. Pantel and C. Alix-Panabieres, *Trends. Mol. Med.* **2010**, *16*, 398-406.

[40] T. Lazarevic, A. Rilak and Z. D. Bugarcic, *Eur. J. Med. Chem.* **2017**, *142*, 8-31.

[41] C. G. Hartinger, S. Zorbas-Seifried, M. A. Jakupec, B. Kynast, H. Zorbas and B. K. Keppler, *J. Inorg. Biochem.* **2006**, *100*, 891-904.

[42] S. Yuan, S. Chen, H. Wu, H. Jiang, S. Zheng, Q. Zhang and Y. Liu, *Chem. Commun.* **2020**, *56*, 1397-1400.

[43] L. I. Rylands, A. Welsh, K. Maepa, T. Stringer, D. Taylor, K. Chibale and G. S. Smith, *Eur. J. Med. Chem.* **2019**, *161*, 11-21.

[44] a) D. Hu, C. Yang, C. N. Lok, F. R. Xing, P. Y. Lee, Y. M. E. Fung, H. B. Jiang and C. M. Che, *Angew. Chem., Int. Ed.* **2019**, *58*, 10914-10918; b) M. Mora, M. C. Gimeno and R. Visbal, *Chem. Soc. Rev.* **2019**, *48*, 447-462.

[45] S. Fruhauf and W. J. Zeller, *Cancer Res.* **1991**, *51*, 2943-2948.

[46] L. Shi, Y. Wang, Q. Wang, Z. Jiang, L. Ren, Y. Yan, Z. Liu, J. Wan, L. Huang, B. Cen, W. Han and H. Wang, *J. Controlled Release* **2020**, *324*, 289-302.

[47] G. Sava, S. Zorzet, C. Turrin, F. Vita, M. Soranzo, G. Zabucchi, M. Cocchietto, A. Bergamo, S. DiGiovine, G. Pezzoni, L. Sartor and S. Garbisa, *Clin. Cancer Res.* **2003**, *9*, 1898-1905.

10.1002/chem.202002970

Table 1. *In vitro* cytotoxicity of ruthenium(II) complexes in comparison with cisplatin. Cells were treated for 72 h, and cell viability was determined by the MTT assay (expressed as IC_{50} ± SD in μM). The ruthenium complexes were dissolved in DMSO and the DMSO contents in culture media were less than 0.2% (v/v) to avoid the solvent impact to cell viability.

	IC_{50} (μM)[a]					
Compounds	A549	A549/cisR	A2780	Huh-7	B16-F10	HUVEC
Ru1	>100	>100	>100	>100	>100	>100
Ru2	94.7±7.7	>100	>100	>100	29.9±4.6	>100
Ru3	80.2±4.3	90.7±3.4	62.2±5.1	84.5±9.1	19.15±5.6	>100
Ru4	35.0±2.4	40.4±2.1	32.7±1.9	97.9±9.3	10.9±1.4	>100
Ru5	28.5±2.2	36.4±1.9	15.5±1.2	81.6±17.6	9.0±1.2	55.7±12.3
Ru6	14.3±1.2	30.9±1.7	11.8±0.7	33.7±4.3	7.3±0.7	38.9±4.9
Ru7	10.3±0.6	19.9±1.5	9.5±0.9	33.1±9.7	5.7±0.8	25.3±3.0
Ru8	4.7±0.4	10.5±0.5	5.1±0.5	15.0±2.5	3.3±0.2	16.2±1.3
Ru9	12.5±1.0	24.9±2.2	22.2±1.6	18.2±1.3	6.9±1.9	28.4±3.3
Ru10	11.5±0.9	23.3±2.2	17.5±1.9	15.7±1.3	4.7±2.0	20.2±2.5
Cisplatin[b]	3.2±0.2	12.5±0.7	2.1±0.06	3.7±0.3	1.3±0.3	8.2±1.0
NAMI-A	>100	>100	>100	>100	>100	>100

[a] IC_{50} = compound concentration required to inhibit tumor cell proliferation by 50%.

[b] A clinical aqueous solution of cisplatin was used as control.

10.1002/chem.202002970

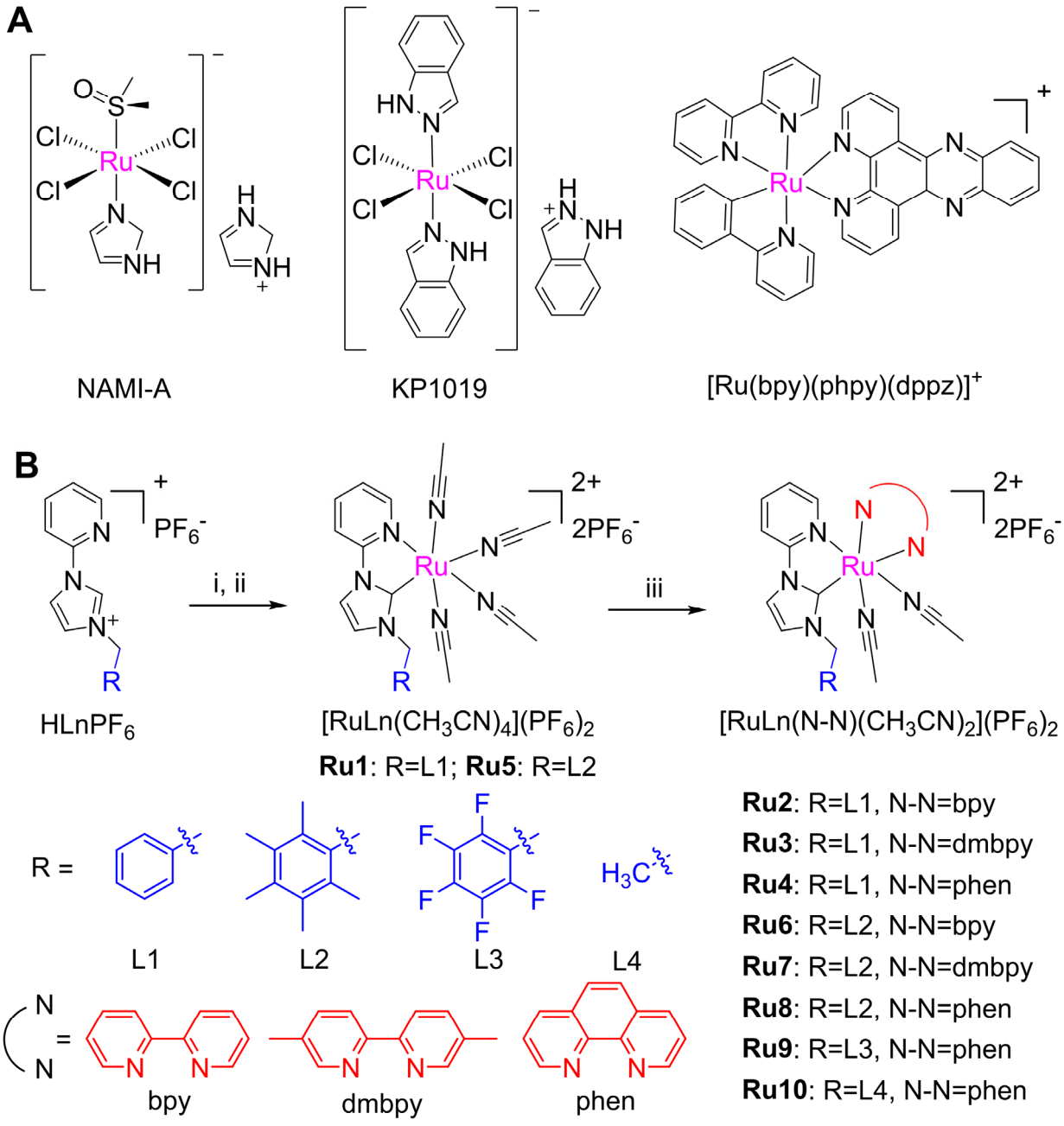

Figure 1. (A) Structures of biologically active ruthenium(II) complexes (NAMI-A, KP1019 and [Ru(bpy)(phpy)(dppz)]$^+$. bpy = 2,2'-bipyridine; phpy = 2-phenylpyridine; dppz = dipyrido[3,2-a:2',3'-c]phenazine). (B) Chemical structures and synthesis of new ruthenium(II) compounds (**Ru1-10**). Reagents and conditions: (i) Ag_2O, CH_3CN, 50 °C, 24 h; (ii) [Ru(*p*-cymene)Cl_2]$_2$, NH_4PF_6, CH_3CN, reflux, 24 h; (iii) N-N ligand (bpy, dmbpy or phen), CH_3CN, reflux, 24 h.

10.1002/chem.202002970

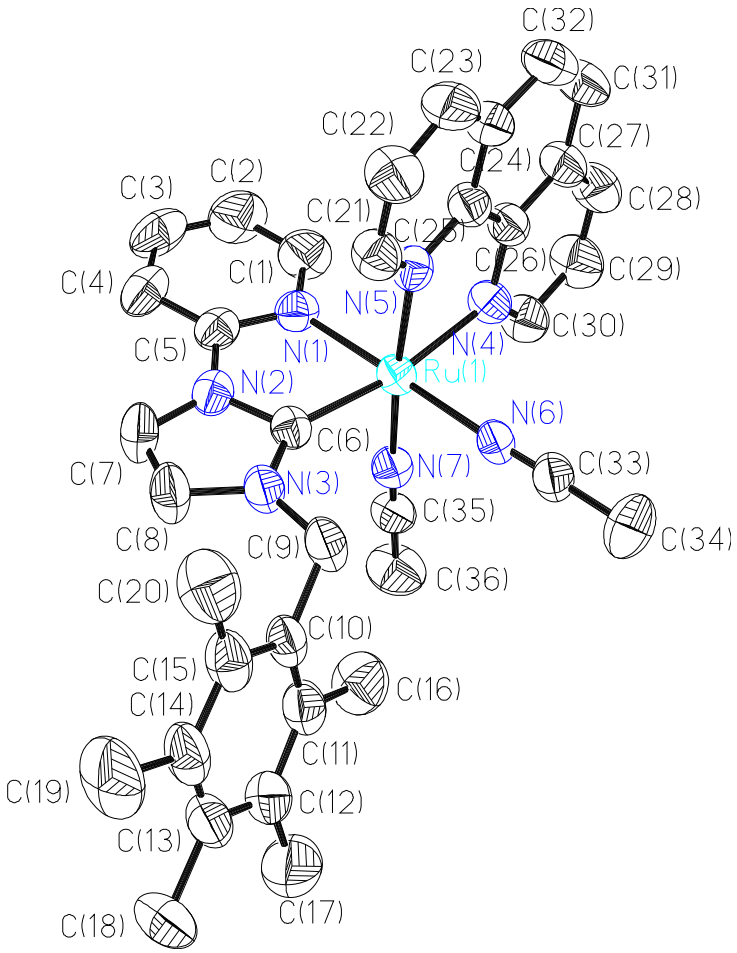

Figure 2. X-ray crystal structure of the complex **Ru8**. Thermal ellipsoid is shown at the 50% probability level.

10.1002/chem.202002970

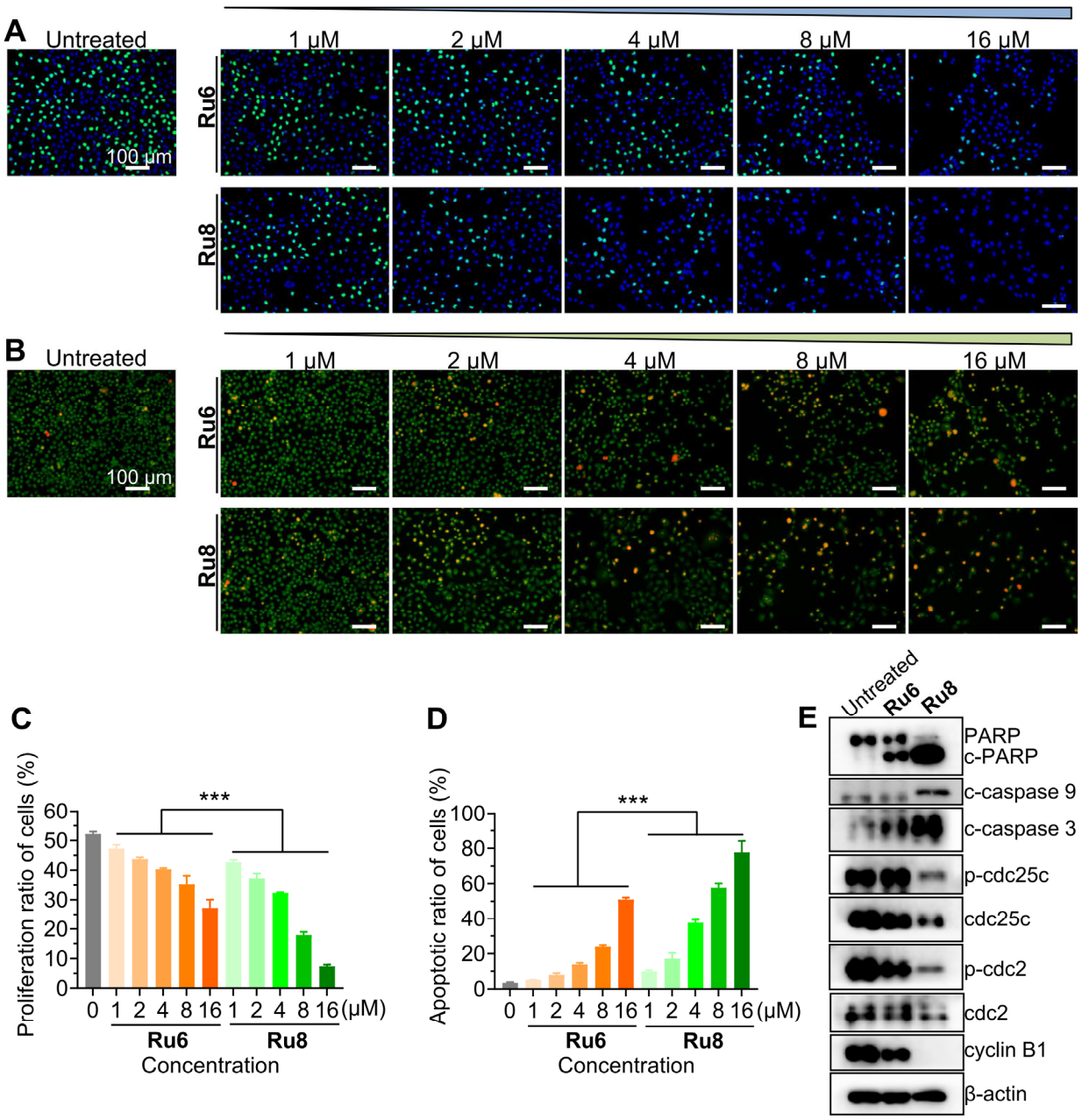

Figure 3. (A) A Click-iT® EdU assay for quantifying the proliferation of A2780 cells. All cells were treated with ruthenium(II) complexes **Ru6** and **Ru8** for 48 h at various concentrations. (B) AO/EB assay quantified the apoptosis of A2780 cells. All cells were treated with **Ru6** and **Ru8** for 48 h at various concentrations. (C-D) Quantification of cell proliferation ratio and apoptosis ratio. Data are presented as the means ± SD for n > 3 regions; ***$p < 0.001$. (E) Western blot analysis of apoptosis- and cell cycle-associated proteins. A2780 cells were treated with the complexes for 48 h.

10.1002/chem.202002970

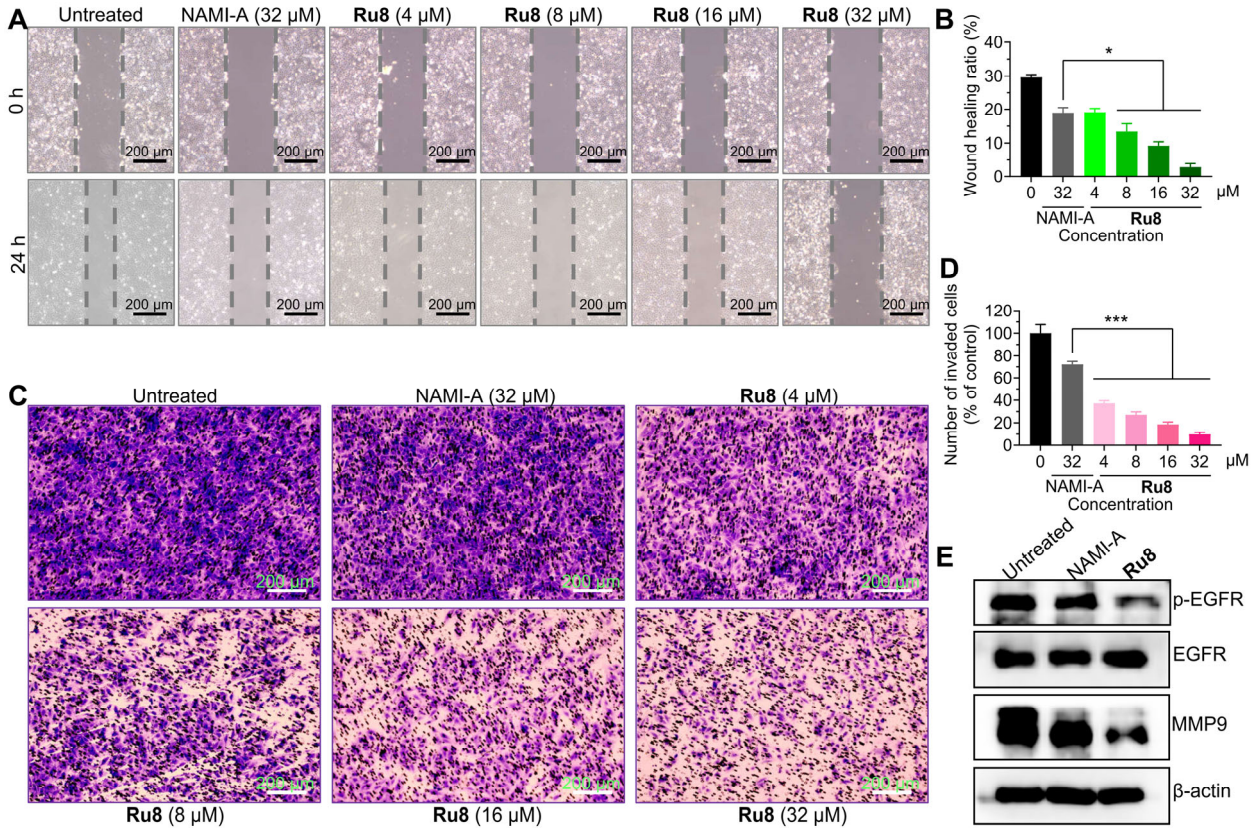

Figure 4. Complex **Ru8** shows antimetastatic activity on cancer cells. (A-B) Wound-healing assay performed on Huh-7 cells. Cells were treated with different concentrations of **Ru8** for 24 h. (C-D) Inhibition of transwell invasion in Huh-7 cells after treatment with different concentrations of **Ru8** for 24 h. Data are presented as the means ± SD for n > 3 regions; **p* < 0.05, ****p* < 0.001. (E) Western blot analysis of metastasis-associated proteins. The cells were treated with NAMI-A and **Ru8** for 24 h.

10.1002/chem.202002970

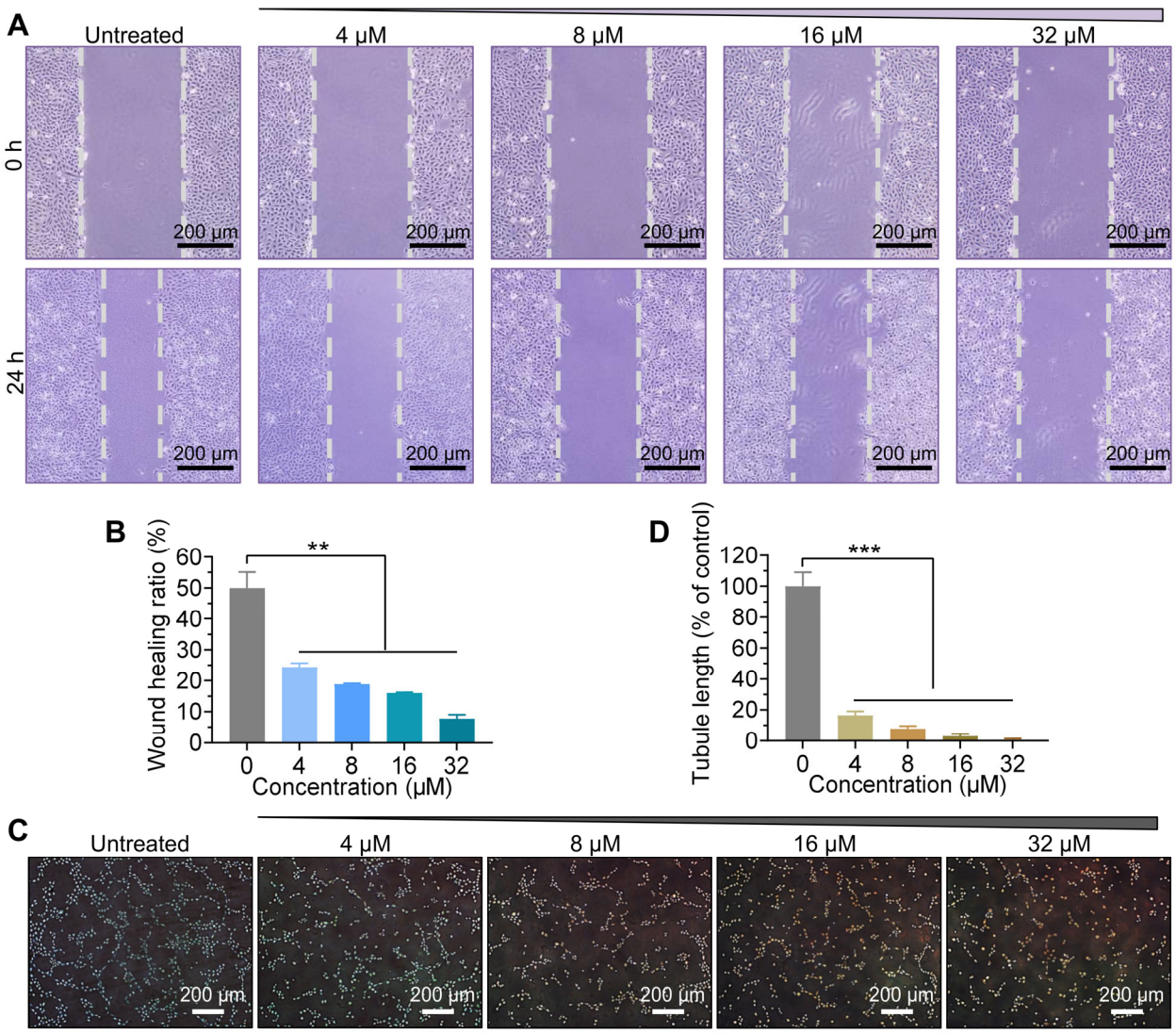

Figure 5. Ru8 shows antiangiogenic activity in cell-based assays. (A-B) Wound-healing assay performed on HUVECs. Cells were treated with different concentrations of **Ru8** for 24 h. (C-D) Inhibition of tube formation in HUVECs after treatment with different concentrations of **Ru8** for 2 h. Data are presented as the means ± SD for n > 3 regions; $^{**}p < 0.01$, $^{***}p < 0.001$.

10.1002/chem.202002970

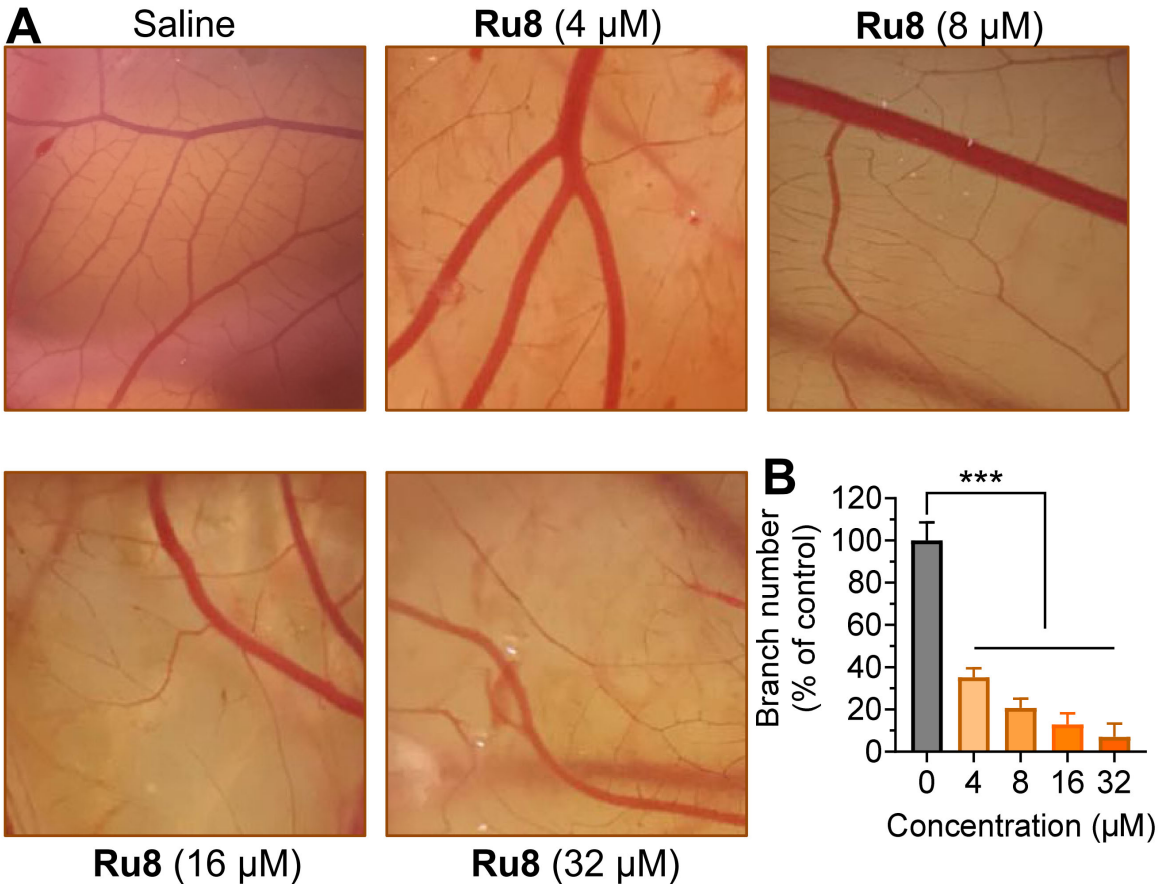

Figure 6. (A) Representative images of the developmental CAM treated with ruthenium(II) **Ru8**. Untreated CAM exhibited small and high dense vessels and capillary network. Treatment with **Ru8** hampered angiogenesis and vessel development in the CAM model. (B) Quantitative analysis of the number of branching points. Data are presented as the means ± SD for n > 3 regions; ***$p < 0.001$.

10.1002/chem.202002970

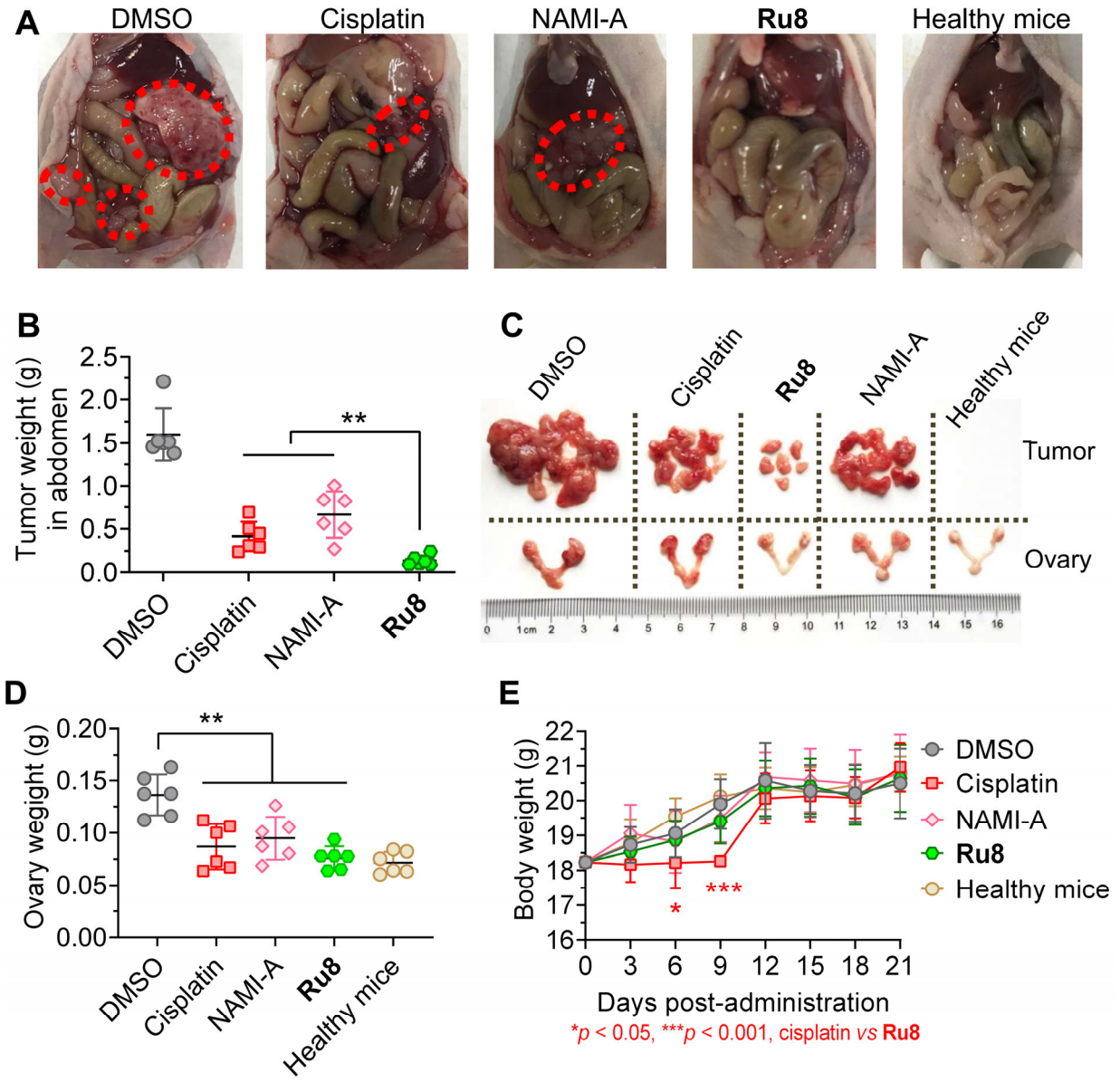

Figure 7. *In vivo* therapeutic efficacy of **Ru8** against metastatic A2780 tumor model. (A) Photographs of tumor-bearing nude mice after different treatments. Healthy mice without tumor cell implantation were used as control. (B) Total abdominal tumor weight excised from the mice after different treatments. Representative images of tumors and ovaries (C), as well as ovary weight (D), in each group at the end of the study. (E) Body weights of mice. Compounds were injected into mice at a dose of 2 μmol/kg every day for one week. Data are presented as the means ± SD; *$p < 0.05$, **$p < 0.01$, ***$p < 0.001$.